FERMILAB-PUB-24-0428-STUDENT

Implementation of a High Resolution Relaxation Measurement and Muon Tagger for coincidence studies ina qubit system.

Charlie Veihmeyer,[1,2] Ryan Linehan,[2] Dylan Temples,[2] and Dan Baxter[2,3]
[1)]*Department of Physics, University of Massachusetts at Amherst, Amherst, MA, 01003, USA*
[2)]*Fermi National Accelerator Laboratory, Batavia, IL 60510, USA*
[3)]*Department of Physics & Astronomy, Northwestern University, Evanston, IL 60208, USA*

(Dated: 1 August 2024)

In this work we explain progress towards a muon tagging system, and associated readout scheme for a flux tunable transmon fabricated on a sapphire chip operated at $\sim$ 15 millikelvin. We explain a measurement system, and the debugging methods implemented. We then begin an introduction to the data analysis chain.

I. INTRODUCTION

Quantum Computing is one of the fastest growing fields in physics, making up a tremendous amount of modern research[1,2]. The shift between classical and quantum computing is in the way that computations are executed, and bits stored. For every classical computation, each bit needs to be individually addressed, and controlled. Quantum computing uses quantum bit, or qubits, the dynamics and interactions of which are governed by quantum mechanics. Physical qubits are often made by isolating the system from it's environment, to the point where the operator can be the dominant influence on it's evolution. In this paper, I will limit our discussion to that of superconducting qubits, and as such will refer to them directly as qubits.

Superconducting qubits come in a variety of forms, though the most common is the transmon. Such a qubit acts as a nonlinear oscillator, using both capacitive and inductive elements. These qubits are typically operated in the Gigahertz range[3]. The flux tunable transmon (see Figure 1) is a type of superconducting qubit which implements a squid loop (2 Josephson Junctions in a loop that gives rise to nonlinear inductance) and a capacitor to create a tunable transmon. The energy of a Josephson loop is as follows:

$$E = -E_j \cos((\delta_0 - 2eVt/\hbar) = -E_j \cos(\phi(t)), \qquad (1)$$

where $E_j = -\frac{\Phi_0 J_c}{2\pi}$. Here Φ_0 is the flux quantum and J_c is the critical current[4]. By tuning the flux through the middle of the Josephson loop, we have control over the energy of the qubit. Superconducting qubits work in extremely low temperatures, $\sim$ 50 mk and lower, to reduce environmental noise and allow us to operate in the quantized energy states of an anharmonic oscillator formed by the qubit potential. In order to get this cold, it is common to use a ^{3}He/^{4}He dilution refrigerator. This work is done in an Oxford Proteox Dilution unit, with a typical operating temperature of 15 mk.

Qubits are fundamentally limited by their error rate, and fault tolerances are typically on the scale of 1% and lower for most surface correction codes[5]. Many modern studies are dedicated to finding the causes of error in these systems[6–8]. It has been observed that qubits can be highly sensitive to environmental sources of decoherence[9].

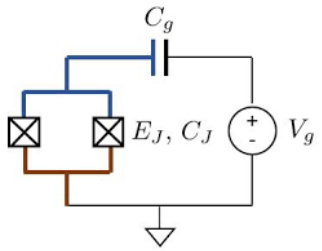

FIG. 1: A circuit diagram of an isolated transmon qubit. This, importantly, does not have any included external components, which are important to the working of a transmon. Figure pulled from Ref. [11]

The sensitivity of qubits to their environmental noise makes them favorable candidates for certain experiments in low energy detection, in particular dark matter. As the WIMP model of Dark Matter has been unfound, many studies are focusing on lighter dark matter candidates, requiring lower energy sensors[10]. Novel strategies to use qubits as particle detectors are being explored Many further studies are needed to create a cohesive story of quantum sensing with qubits, but initial measurements show optimistic results of having flexible systems capable of multiple low energy measurements.

In this work, I describe steps taken towards understanding and improving qubit relaxation response to cosmic ray interactions in the substrate, in particular in Niobium. In the next section, I will discuss a muon detector that we aim to use to detect coincidence events, confirming that we are seeing muons. After this, we will briefly discuss the theoretical impact of quasiparticle population on the qubit relaxation rate. In Section II, we will explain the measurement procedure, and the methods that we have taken to ensure that it is working as intended. In the last Section, we will discuss the statistical analysis we do on the data.

A. Muon Detection

The analog electronics for a muon tagger were created by Simon Mork[12], a previous SULI intern, and now graduate student at the university of Arizona. It fundamentally works with three scintillating paddles, each of which is connected to it's own photo-multiplier tube. A scintillator is a material that emits photons when hit with high energy particles or photon. This light emission is then detectable by a photo-multiplier tube, which acts as a counter of photons. When a muon or other particle interacts with a scintillating paddle, the interaction releases light. This light is then funneled towards the photo-multiplier tube by a waveguide. This photo-multiplier tube acts as a converter from the photon to an electrical signal, which is detectable by a readout system. Converting this pulse into a measurable output is done by a set of nuclear instrumentation modules, or NIM. The NIM electronics determine coincidence between the three paddles, and send a pulse to a Raspberry Pi equipped with a MCC 128 DAQ HAT. The Raspberry Pi records a timestamp for each pulse it receives, indicating a coincidence between the three paddles was detected. For a discussion of the false rate of these paddles, please see Ref. 12. More details on the NIM electronics can be found in Appendix A.
The electronics chain leaves us with a timing resolution of approximately 115 μs for the timestamps, with the limiting factor being the sampling rate of the MCC 128 DAQ HAT.

The three scintillating paddles are supported in a stand underneath the refrigerator. The paddles are held at 7 and 5 inches apart, and close to the bottom of the refrigerator, and the top paddle is 4 inches underneath the refrigerator, as can be seen in Figure 2.

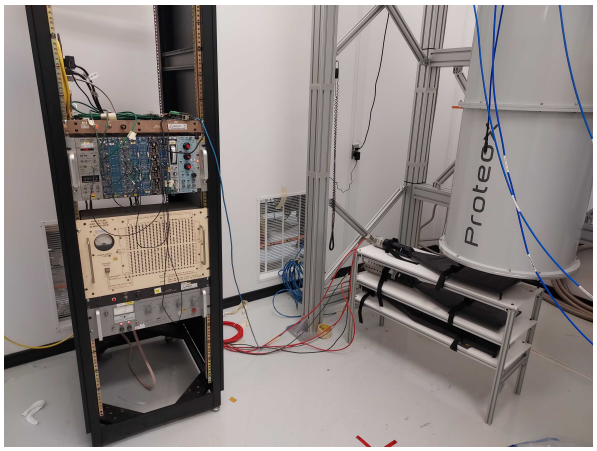

FIG. 2: An image of the muon paddles underneath the refrigerator in our lab space. We

B. Quasiparticle Poisoning in qubits.

Quasiparticle interactions within qubits, and in particular Josephson Junctions, are a significant source of error in quantum circuits. A common error is a relaxation error is a loss of the qubit state prior to completion of all desired operations. Qubits have a typical time it takes for them to decay, which we will refer to as the relaxation time. Quasiparticles cause a much higher rate of relaxation errors. This can be explained by a microscopic picture, where a quasiparticle takes the energy from a qubit to tunnel across the potential barrier formed by the Josephson Junction, causing the qubit to go from it's excited state to it's ground state.

This relaxation time follows the form

$$\Gamma = \Gamma_{qp} + \Gamma_{other}, \tag{2}$$

where $\Gamma = 1/T_1$ is the relaxation rate, T_1 is the relaxation time, Γ_{qp} is contribution from quasiparticles, and Γ accounts for other sources of error within the system[6]. This is an attribute of the qubit, which indicates how long it will remain excited after initial excitement. For this measurement, our qubit has a relaxation time of 4-5 μs. The quasiparticle relaxation rate follows the form:

$$\Gamma_{qp} = \sqrt{\frac{2\omega_q \Delta}{\pi^2 \hbar}} x_{qp} \tag{3}$$

where ω_q is the frequency of the qubit, Δ is the superconducting gap of the qubit material, and x_{qp} is the normalized quasiparticle density[6]. The creation of phonons in a solid state medium, on top of which a qubit lives, causes increased error rates in the qubit. It is well established that the density of quasiparticles is higher than expected for superconductors operating at milikelvin temperatures[9]. Studies of this show that non-equilibrium quasiparticles are produced by ionizing radiation[6], microscopic mechanical stresses[13], and cosmic rays[8], and subsequent work is being done to reduce the impact of these events in qubit chips.

Additional studies have been done to understand the sensitivity of these qubits, aiming towards implementing qubits as a detector of quasiparticle population. For any event creating phonons, if the phonon energy is above 2Δ then these phonons are capable of breaking cooper pairs. This generates quasiparticles, which may lead to a increase in qubit decoherence[10]. In this way, it is believed that qubits could be implemented as quasiparticle detectors. The work in this paper is a description of progress towards an experimental system allowing further studies, operating with a similar detection principal as in Harrington et al[8].

II. OPERATING QUBITS IN RELAXATION MODE

Of central interest to this project is operating our qubits in a measurement mode sensitive to slight changes in the qubits relaxation time. Previous studies have searched for similar interactions, however this will be the first time that this study is done with a Niobium qubit on Sapphire, as opposed to Aluminum on Silicone. Our goal is to detect muons, and work to understand the underlying physics that would allow us to be

either less or more sensitive to these interactions. For our purposes, we require a high sampling rate to detect muon events, based on simulations[10], where they find that muon events in the substrate will create a detectable change in error rate for approximately a millisecond. To do this, we need to use a measurement circuit which gives us a high timing resolution, which requires a single shot readout.

Important for this measurement is a good single shot readout. Single shot readout is when we assign a threshold to dispersive readout[14]. We tune our single shot measurement in the following way: We first prepare the ground state and measure N times. We then prepare the excited state and measure N times. Plotting these values, we identify a threshold which gives us the highest single shot fidelity. The single shot fidelity is $1-P_{eg}-P_{ge}$, where P_{eg} is the probability that we measure e after preparing the qubit in ground, and P_{ge} is the probability we measure ground after preparing an excited state. This measurement is the data that is used to generate plot b in Figure 4. After this step, we can proceed to the relaxation measurement.

We first use a π pulse to place the qubit in the excited state (see appendix for details on qubit). After waiting a time τ, we measure the qubit state, after which we wait a period of time allowing the qubit to decay back to ground. A schematic of this experiment can be seen in Figure 3. This measurement procedure was first implemented by Harrington et al[8].

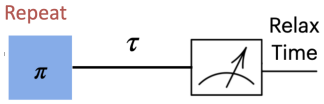

FIG. 3: The measurement we are attempting to use to search for anomalous decay errors. By sweeping τ and the relax delay, we can find a point with the highest baseline, while still being sensitive to relaxation events.

An effective logic check, ensuring that the qubit measurement is performing as expect, is executed by varying τ. As τ is the time after the π pulse, before the measurement, the qubit should decay more often the longer τ is. Our analysis for this data involved taking 200000 measurements, and then averaging them together to create a baseline. This measurement takes data for 6.8 seconds. We assume that each measurement has the same likelihood of relaxation errors, and therefore calculate the average of the measurement as a baseline, and use it to describe the expected error rate.

To confirm that our measurement is behaving as expected, we want to calculate the baseline using probabilities from an independent measurement. To calculate this we use specific statistics gathered from Figure 4,

$$\begin{aligned} P_b = {} & P_{exc}e^{-\Gamma t}P(e|g) + P_{exc}(1-e^{-\Gamma t})P(e|g) \\ & + (1-P_{exc})e^{-\Gamma t}P_d P(e|e) + (1-P_{exc})e^{-\Gamma t}(1-P_d)P(e|g) \\ & + (1-P_{exc})(1-e^{-\Gamma t})P(e|g), \quad (4) \end{aligned}$$

where P_b is the chance that, for any given measurement, the qubit is either excited, after using a pi pulse. Here P_{exc} is the

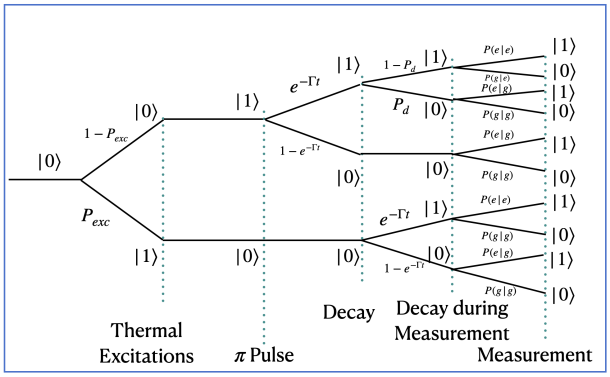

(a) This figure demonstrates the probability tree that we use to calculate the baseline measurement. Each node with more than one daughter is an event which is represented with the dotted line. Dotted line intersections with no node indicate that the event is either not considered, or it is a process impossible to apply to the qubit state. At each point, we include the probability that a certain event occurs. In order to find our baseline, we take the product of each line that ends in the qubit state as 1.

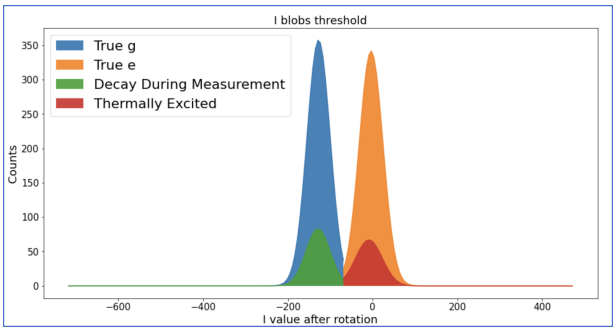

(b) We first prepare the qubit state in ground, and measure. We then prepare it in excited state and measure, the same number of times as we measured in ground. We read these values using dispersive readout, and the measured value is the power of the 0-phase resonator pulse. When our qubit is in it's excited state, it causes this power to increase, while it is lowered in it's ground state. After assigning a threshold to distinguish between states, we can see when, after preparing in one state, we measure the other, as exampled by the green and red plots. We generate histograms of this data, and fit to it, and it is these fits that are plotted. Our measurement of and $P(e|g)$, $P(g|e)$, and thermal excitation and probability of decaying during measurement is gained from this plot. See text for details on extracting these values.

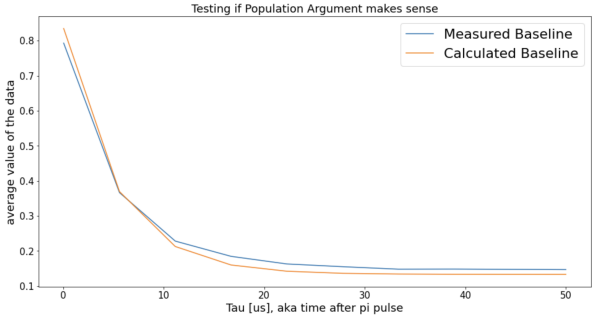

(c) This plot demonstrates a sweep over τ, where we follow the model as described in the text in Section II. Importantly, this is an approximation, where we assume the rate of excitation error is the same as the rate of de-excitation errors.

FIG. 4

probability the qubit is thermally excited, P_d is the probability the qubit does decays, and $P(e|g)$ are direct measurement probability's. In order to calculate each of these, we refer to figure 4. We assign a threshold to these measurement, based on our prepared state of ground vs excited. Below this value, any value that is recorded will be considered ground, and all values above it will be considered excited.

We normalize by the full area from each measurement cycle, meaning that each probability comes from the area of the Gaussians divided by the sum of the area under each cases Gaussians. In example, the probability of being thermally excited is the area of the red Gaussian divided by the sum of the area in 'True g' and the 'Thermally Excited' Gaussian.

P_{exc} is the area under the red Gaussian, and refers to the thermally excited state, meaning states that are excited by environment, not by us.

$P(e|g)$ is the tail (not shown in figure 4) of the Gaussian that extends across the threshold, and $P(g|e)$ is the tail of the orange blob, extending across the threshold. Both of these refer to the probability that the measurement itself is wrong, and the qubit state is truly g or e, respectively. P_d is the area of the green blob minus the area of the red blob, the likelihood that the qubit decays during the measurement. We have to subtract the area of the red plot, as this is resident thermal population. $P(e|e)$ is found by doing $1 - P(g|e)$, as we are assuming that the qubit is not excited beyond it's first excited state ever. This is similarly how we calculate $P(g|g)$.

It is important to use the same readout measurement length for this measurement as the one where we sweep τ, in order to keep the probability that this decays consistent. Additionally, it should be clear that this is purely an approximation of the true probabilities, and we used only a first order model with an important assumption, in order to generate an approximate result.

This is the probability that the qubit was excited before measurement. The calculated curve, as seen in Figure 5 is accurate, to first order approximations. This test is not fully capable of avoiding specific qubit difficulties, but offers a channel to logically test the procedure without intensive reliance on a low-noise system. With some minor reassurance that measurement was working as intended, we proceeded to begin to measure, and discuss our initial measurement and data anlysis procedures.

A. Waveforms

For relaxation mode, we execute the measurement circuit 200000 times, corresponding to 200000 measurements and 6.8 seconds of live time. In order to figure out how long we would need to measure to detect a muon event, we first assume that all muon flux is vertical. While this is an untrue assumption, it is unlikely to greatly reduce the rate of muons, as we have sensitivity to about 30 degrees from the azimuth, incident on the qubit. The muon flux is, according to our detector, 9.8 per second. We have an effective measuring area of 90 in^2, so we have .108 muons per square inch per second. We

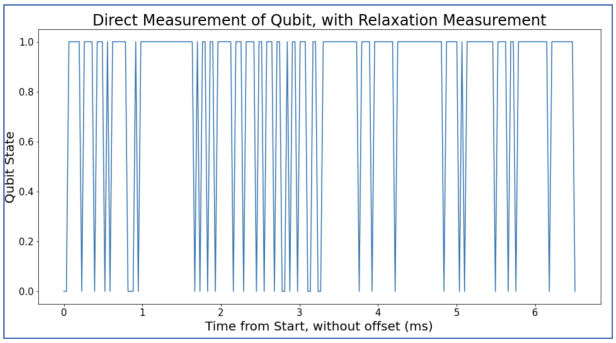

FIG. 5: An example of the qubit time stream we get from the measurement. Full data set not pictured.

can then relate this to our qubit chip, which has a size of 64 mm^2. This calculation tells us that the muon flux through the chip is .01 per second. Realistically, this means that we have a collision once every 2 minutes. However, we strongly suspect that due to our fidelity (measurement accuracy), we will need interactions to be much closer on the chip, as opposed to any where on the chip. Operating with an effective area of a 1mm radius around the qubit, we would have 1-2 collisions per hour. This measurement has not yet been done, as we are still creating the data processing software. When measuring, we get a time stream of qubit states, as seen in figure 5.

Timing accuracy of the measurement is of high importance, especially when considering coincident events. In order to achieve relative timing accuracy, every time a measurement is executed from QICK: a Xilinx RFSoC board with custom open-source software and firmware for the control of qubit systems[15], it triggers a channel which is then recorded on the same DAQ HAT that is on the Raspberry Pi. In doing this, we are able to correlate measurement times versus muon interaction times. We have, as yet, been unable to demonstrate this capability.

III. CONCLUSION

In this work, we show progress towards correlating events in a muon detector with qubits operated in a relaxation rate sensitive readout. The current state of the project is in developing methods for analysis of the data, and improving readout to be more efficient. Due to this inefficiency of data collection, we have yet to operate both the qubit measurement, and the muon detector with the intent of coincidence detection between them. Future work will aim to to do this in addition to studying this process with greater depth.

IV. ACKNOWLEDGEMENTS

This manuscript has been authored by Fermi Research Alliance, LLC under Contract No. DE-AC02-07CH11359 with the U.S. Department of Energy, Office of Science, Office of High Energy Physics. This work was supported in part by

the U.S. Department of Energy, Office of Science, Office of Workforce Development for Teachers and Scientists (WDTS) under the Science Undergraduate Laboratory Internships Program (SULI). This work was supported by the U.S Department of Energy, Office of Science, National Quantum Information Science Research Centers, Quantum Science Center and the U.S. Department of Energy, Office of Science, High-Energy Physics Program Office.

[1] J. P. Dowling and G. J. Milburn, "Quantum technology: The second quantum revolution," (2002), arXiv:quant-ph/0206091 [quant-ph].

[2] M. A. Nielsen and I. L. Chuang, *Quantum Computation and Quantum Information* (Cambridge University Press, 2000).

[3] J. Koch, T. M. Yu, J. Gambetta, A. A. Houck, D. I. Schuster, J. Majer, A. Blais, M. H. Devoret, S. M. Girvin, and R. J. Schoelkopf, "Charge-insensitive qubit design derived from the cooper pair box," Physical Review A **76** (2007), 10.1103/physreva.76.042319.

[4] B. D. Josephson, "The discovery of tunnelling supercurrents," Rev. Mod. Phys. **46**, 251–254 (1974).

[5] A. N. Cleland, "An introduction to the surface code," SciPost Phys. Lect. Notes , 49 (2022).

[6] A. P. Vepsäläinen, A. H. Karamlou, J. L. Orrell, A. S. Dogra, B. Loer, F. Vasconcelos, D. K. Kim, A. J. Melville, B. M. Niedzielski, J. L. Yoder, S. Gustavsson, J. A. Formaggio, B. A. VanDevender, and W. D. Oliver, "Impact of ionizing radiation on superconducting qubit coherence," Nature **584**, 551–556 (2020).

[7] C. D. Wilen, S. Abdullah, N. A. Kurinsky, C. Stanford, L. Cardani, G. D'Imperio, C. Tomei, L. Faoro, L. B. Ioffe, C. H. Liu, A. Opremcak, B. G. Christensen, J. L. DuBois, and R. McDermott, "Correlated charge noise and relaxation errors in superconducting qubits," Nature **594**, 369–373 (2021).

[8] P. M. Harrington, M. Li, M. Hays, W. V. D. Pontseele, D. Mayer, H. D. Pinckney, F. Contipelli, M. Gingras, B. M. Niedzielski, H. Stickler, J. L. Yoder, M. E. Schwartz, J. A. Grover, K. Serniak, W. D. Oliver, and J. A. Formaggio, "Synchronous detection of cosmic rays and correlated errors in superconducting qubit arrays," (2024), arXiv:2402.03208 [quant-ph].

[9] C. Wang, Y. Y. Gao, I. M. Pop, U. Vool, C. Axline, T. Brecht, R. W. Heeres, L. Frunzio, M. H. Devoret, G. Catelani, L. I. Glazman, and R. J. Schoelkopf, "Measurement and control of quasiparticle dynamics in a superconducting qubit," Nature Communications **5** (2014), 10.1038/ncomms6836.

[10] R. Linehan, I. Hernandez, D. J. Temples, S. Q. Dang, D. Baxter, L. Hsu, E. Figueroa-Feliciano, R. Khatiwada, K. Anyang, D. Bowring, G. Bratrud, G. Cancelo, A. Chou, R. Gualtieri, K. Stifter, and S. Sussman, "Estimating the energy threshold of phonon-mediated superconducting qubit detectors operated in an energy-relaxation sensing scheme," (2024), arXiv:2404.04423 [physics.ins-det].

[11] J. Chávez-Garcia, F. Solgun, J. Hertzberg, O. Jinka, M. Brink, and B. Abdo, "Weakly flux-tunable superconducting qubit," (2022).

[12] S. D. Mork, L. Hsu, P. T. Lukens, and D. J. Temples (NEXUS), "Implementation of a Time-domain Cosmic-ray-muon Tagger for the NEXUS Low-background Cryogenic Facility," .

[13] R. Anthony-Petersen, A. Biekert, R. Bunker, C. L. Chang, Y.-Y. Chang, L. Chaplinsky, E. Fascione, C. W. Fink, M. Garcia-Sciveres, R. Germond, W. Guo, S. A. Hertel, Z. Hong, N. Kurinsky, X. Li, J. Lin, M. Lisovenko, R. Mahapatra, A. Mayer, D. McKinsey, S. Mehrotra, N. Mirabolfathi, B. Neblosky, W. A. Page, P. K. Patel, B. Penning, H. D. Pinckney, M. Platt, M. Pyle, M. Reed, R. K. Romani, H. S. Queiroz, B. Sadoulet, B. Serfass, R. Smith, P. F. Sorensen, B. Suerfu, A. Suzuki, R. Underwood, V. Velan, G. Wang, Y. Wang, S. L. Watkins, M. R. Williams, V. Yefremenko, and J. Zhang, "A stress induced source of phonon bursts and quasiparticle poisoning," (2022), arXiv:2208.02790 [physics.ins-det].

[14] P. Krantz, M. Kjaergaard, F. Yan, T. P. Orlando, S. Gustavsson, and W. D. Oliver, "A quantum engineer's guide to superconducting qubits," Applied Physics Reviews **6** (2019), 10.1063/1.5089550.

[15] L. Stefanazzi, K. Treptow, N. Wilcer, C. Stoughton, C. Bradford, S. Uemura, S. Zorzetti, S. Montella, G. Cancelo, S. Sussman, A. Houck, S. Saxena, H. Arnaldi, A. Agrawal, H. Zhang, C. Ding, and D. I. Schuster, "The qick (quantum instrumentation control kit): Readout and control for qubits and detectors," Review of Scientific Instruments **93** (2022), 10.1063/5.0076249.

[16] K. Ramanathan, J. E. Parker, L. M. Joshi, A. D. Beyer, P. M. Echternach, S. Rosenblum, B. J. Sandoval, and S. R. Golwala, "Quantum parity detectors: a qubit based particle detection scheme with mev thresholds for rare-event searches," (2024), arXiv:2405.17192 [physics.ins-det].

Appendix A: Muon Monitor Detail

Much of this information comes directly from reference 12, and was completed by a previous SULI interned, Simon Mork. Simon is now a graduate student at the University of Arizona, and his work was instrumental in constructing the analog electronics behind the muon monitor. This will only be a brief summary of the electronics of the system, for more detail please refer to Ref. 12.

The system works with three scintillating paddles connected to photomultiplier tubes, which are powered at ~ -2000 volts. Each signal is plugged into a Lecroy Model 428F linear fan-in/fan-out module, which allows for multiple outputs, for future timing tuning. The LeCroy Model 623 Octal Discriminator converts the pulses from analog to digital by scanning for a rising edge pulse of -30 mV, and returns a logic pulse with an amplitude of $\sim$ 800 mV. This pulse is fed into a LeCroy Model 365 4-fold Logic Unit, which determines logical coincidence of these pulses. Of additional importance is the inclusion of a 10 ns coincidence time, which is set to reduce the chance of false coincidences. This pulse is sent to a Phillips Model 795 Quad Gate/Delay Generator to generate a NIM pulse of much wider width, which is detectible by a MCC 128 DAQ HAT attached to a Raspberry Pi, which records this logic pulse.